Tunable flow asymmetry and flow rectification with bio-inspired soft leaflets

M. Brandenbourger, * A. Dangremont, R. Sprik, and C. Coulais
Institute of Physics, Universiteit van Amsterdam, Science Park 904, 1098 XH Amsterdam, Netherlands

(Received 1 November 2019; revised 7 May 2020; accepted 1 July 2020; published 10 August 2020)

In nature, liquids often circulate in channels textured with leaflets, cilia, or porous walls that deform with the flow. These soft structures are optimized to passively control flows and have inspired the design of novel microfluidic and soft-robotic devices. Yet, the relationship between the geometry of the soft structures and the flow properties remains so far poorly understood. Here, taking inspiration from the lymphatic system, we devise millifluidic valves, dressed with asymmetric soft leaflets that feature on-demand asymmetric flow properties, which we harness to induce flow rectification and pumping. We demonstrate that the functional mechanism at play involves an interplay between geometry, asymmetry, and fluid-structure interaction-induced nonlinearity. Our results open the way to a better characterization of biological leaflet malformations and to more accurate control of flows for microfluidics and soft-robotic systems.

DOI: 10.1103/PhysRevFluids.5.084102

I. INTRODUCTION

Every living system is composed of soft elements containing fluids [1]. In many cases, these fluids circulate within the living body to transport functional fluids such as blood or lymph via a variety of fluid-structure interactions [1–8] and pumping mechanisms [1–4]. One particularly robust mechanism to transport fluids at low Reynolds numbers takes place in the lymphatic system. The specificity of lymphatic valves lays in their unique shape and arrangement allowing for a very efficient way to passively create unidirectional flows. Soft and asymmetric leaflets distributed along the lymphatic channel promote forward flows rather than backward flows at any flow rate [3]. This flow asymmetry, coupled with self-regulated contractions of muscles surrounding the lymphatic channel [5], induces distributed pumping along the lymphatic channel. Although flow-response asymmetry has been described as a consequence of a nonlinear interaction between a laminar flow and deformable asymmetric leaflets [3,9–16], our understanding of the relationship between the flow unidirectional response and the leaflets' geometry and mechanics remains limited to empirical models [3,17].

Here, inspired by the lymphatic system [3,5,17], and building on the field of fluid-structure interaction of flexible structures [3,9–16], we establish how flow asymmetry (i) emerges from an interplay between geometric asymmetry and nonlinearity induced by a fluid-structure interaction, and (ii) can be used to induce flow rectification, thus passively converting an oscillatory flow into a net fluid transport. The paper is organized as follows. We first demonstrate that realistic bio-inspired channels exhibit a nonlinear and asymmetric flow response. Next, we rationalize these results by performing experiments and simulations on a simplified geometry retaining only the essence of the fluid-structure interaction. This allows us to develop an analytical model that provides design guidelines to maximize the flow asymmetry using soft leaflets. We then evidence

*Corresponding author: martinbdbg@gmail.com

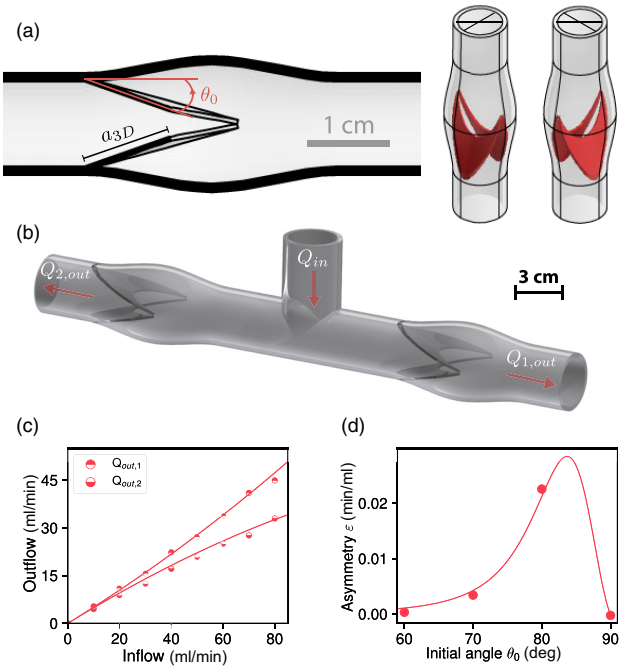

FIG. 1. 3D printed lymphatic leaflet. (a) Schematic of a 3D valve leaflet inspired from 3D scanners of lymphatic leaflets [6]. (b) Schematic of the setup mimicking two lymphatic valves in a T-junction geometry. (c) Outflows $Q_{\text{out},1}$ and $Q_{\text{out},2}$ as a function of the inflow Q_{in} for an initial opening $\theta_0 = 70°$. For each inflow Q_{in}, $Q_{\text{out},1} > Q_{\text{out},2}$. The red line corresponds to a fit given by Eq. (1). (d) Flow asymmetry ε vs initial leaflet angle θ_0. The red line corresponds to a fit from the analytical expression of ε obtained from Eq. ([1]).

experimentally the existence of an optimum valve geometry where the flow asymmetry is maximal. Finally, we demonstrate that such leaflets can be used to rectify flow oscillations and induce pumping. Our findings provide design guidelines for designer fluidics that could be woven with microfluidics [10,14,18–20], soft robotics [21–26], and bioprinting [27], as well as provide insights on malfunctions of lymphatic valves [3,17].

II. RESULTS

A. Lymphatic leaflets' geometry

Figure 1(a) shows the schematics of a three-dimensional (3D) printed soft valve inspired by 3D scanners of lymphatic leaflets [6]. The valve is composed of two soft leaflets connected to the side of the channel. As in lymphatic systems [3,6], the valve is open at rest. Its aperture is defined by the initial angle θ_0 and the length a_{3D}(see Fig. 1(a) and the Supplemental Material [28] for further descriptions). The valve was printed out of elastic material (Young's modulus 1 MPa; see the Supplemental Material [28]) and scaled up by a factor of 15. To capture the influence of the leaflets on the flow under controlled conditions, we created a T-shaped channel, with one inlet and two outlets, where two leaflets are placed between the inlet and each outlet [see Fig. 1(b)]. We filled the channel with silicone oil of viscosity 1 Pa s, which guaranties a Reynolds number of $\text{Re} < 10^{-1}$ that is comparable to Reynolds numbers involved in secondary lymphatic valves [3]. We performed the experiments as follows: we impose the incoming flow rate Q_{in} using a syringe pump and measure the flow rate of the two outlets $Q_{1,\text{out}}$ and $Q_{2,\text{out}}$.

The measurements shown in Fig. 1(c) indicate a nonlinear inflow-outflow relation for both outlets. For any inflow Q_{in} the outflow from outlet 1, $Q_{1,\text{out}}$ is higher than the outflow for outlet 2, $Q_{2,\text{out}}$. To quantify this asymmetry, we expand the nonlinear pressure difference between inlet and outlet to quadratic order

$$\Delta p = R\, Q\, (1 + \varepsilon Q), \tag{1}$$

where R, the flow resistance of the channel, and ε, the asymmetry of flow, depend on the leaflet geometry and orientation. In contrast with other models describing physiological flows [29], the quadratic expansion allows us to quantify explicitly the flow asymmetry ε (see the Model section below). In addition, we will derive such quadratic expansion from first principles to obtain a prediction of R and ε based on the leaflets' geometry. We use Eq. (1) to derive expressions of the outflows $Q_{1,\text{out}}$ and $Q_{2,\text{out}}$ as a function of Q_{in} (Supplemental Material [28]) and fit them to the experimental data [Fig. 1(c), red lines). The result characterizes well the asymmetry observed in Fig. 1(c) and allows us to quantify the value of the asymmetry ε. Crucially, this set of experiments demonstrates that a net flow is always induced in the right direction with a flow rate $\delta Q = \varepsilon Q_{\text{in}}^2/2$ (see the Supplemental Material [28]) that is controlled by the inflow, and which, as we will show at the end of the paper, provides a robust mechanism for flow rectification and thus fluid transport.

Next, we show that the flow asymmetry can be optimized by the leaflets' geometry. We performed the same experiments for four pairs of valves with different initial angles $\theta_0 = 60°$, 70°, 80°, 90° and plotted in Fig. 1(d) the flow asymmetry ε vs the initial angle θ_0. While channels with very tilted ($\theta_0 = 60°$) or straight leaflets ($\theta_0 = 90°$) exhibit very small flow asymmetry, channels with moderately tilted leaflets ($\theta_0 = 70°$ and 80°) exhibit a relatively larger flow asymmetry. This result indicates the existence of a fine balance between the geometric asymmetry of the leaflets and their interaction with the flow that allows for an optimum geometry maximizing flow asymmetry. However, the complex 3D geometry of the valve prevents the precise analysis of the valve deformation and therefore limits the conclusions and further studies on the geometric parameters governing the asymmetry. Therefore, in the remainder of the paper we will focus on an idealized version of the lymphatic leaflets that have an extruded two-dimensional (2D) shape, which will allow us to easily quantify the leaflet deformation with the flow.

B. 2D leaflets geometry

Using 3D printing, we create bio-inspired soft valves made of two soft leaflets placed on each side of a channel filled with a water-glycerol mixture of viscosity $\eta = 0.3 \pm 0.05$Pa s [Fig. 2(a)]. The two leaflets are made of a soft (Young's modulus $E_{\text{leaflet}} = 2$ MPa) or a rigid (Young's modulus $E_{\text{leaflet}} = 3$ GPa) material, while the channel surrounding the leaflets is rigid (Young's modulus $E_{\text{channel}} = 3$ GPa). The leaflets' height is 1.8 mm, slightly smaller than the channel's height of 2 mm, and are positioned in the center of the channel, such that they can freely bend without touching the channel's walls. We apply a constant flow rate using a syringe pump, and restrict our attention to flow rates $|Q| \leqslant 80$ ml/min, which guarantees a Reynolds number $\text{Re} < 10^{-1}$ and therefore a laminar flow. The pressure was measured at two points, on both sides of the leaflets. The new leaflet geometry allows us to track their deformation with the flow. While backward flows (–80 and –40 ml/min) largely reduce the gap for the liquid to flow, forward flows (40 and 80 ml/min) slightly increase the gap between both leaflets [Fig. 2(b)]. We first measure the average deflection of the two leaflets as a function of the applied flow rate for both rigid and soft valves. As expected, the rigid leaflets [Fig. 2(c), blue circles] do not deform with the flow. In contrast, the soft leaflets deviate linearly from their initial angle θ_0 [Fig. 2(c), red circles]. At high backward flows, the angle θ varies rapidly as the gap between the leaflets reduces. The deformation of the leaflets has a direct influence on the geometry of the channel, which in turn affects the pressure drop ΔP induced by the leaflets. For rigid leaflets, ΔP evolves linearly with the flow rate [Fig. 2(d), blue circles], which is consistent with the fact that the flow is laminar and that the leaflets are immobile. In contrast, for soft leaflets the pressure ΔP evolves nonlinearly with the flow rate Q [Fig. 2(d), red circles]. As the

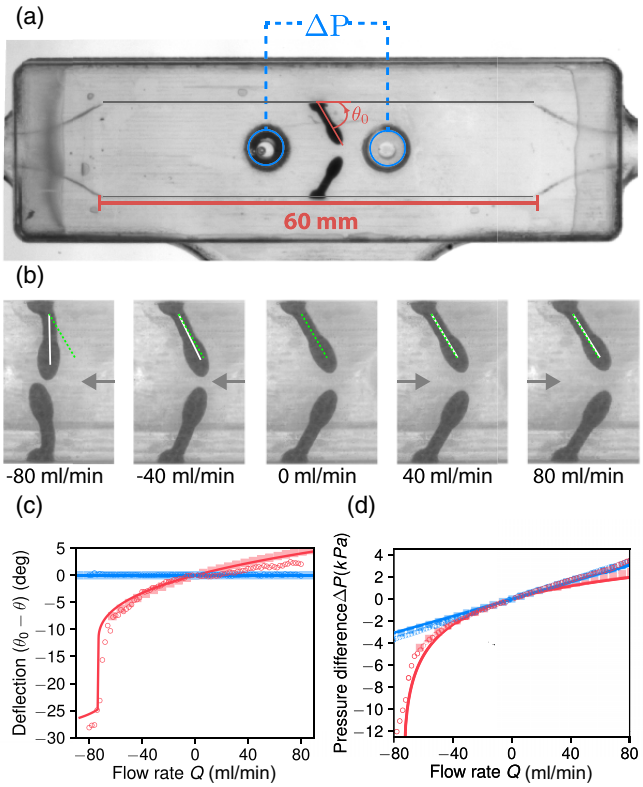

FIG. 2. leaflets geometry. (a) A pair of 2D soft leaflets at an angle $\theta_0 = 60^\circ$ in a rectangular rigid channel. The two holes highlighted in blue are connected to two pressure sensors. (b) Close-up on the soft leaflets for different backward and forward flow rates. (c) Average deflection $\theta - \theta_0$ of rigid leaflets (in blue) and soft leaflets (in red) vs flow rate Q. (d) Pressure difference ΔP measured on each side of the valve vs flow rate Q for rigid leaflets (in blue) and soft leaflets (in red). The open circles, squares, and continuous lines correspond, respectively, to the experiments, the finite element simulations, and the model.

flow rate increases toward positive (negative) values, the pressure difference increases (decreases) slower (faster) than the rigid leaflet case. In other words, the leaflet deformations do not only lead to nonlinearities but also to an asymmetry in the pressure-flow relationship. This asymmetry is even more pronounced at high backward flows where the pressure diverges similarly to the deflection of the leaflets. Importantly, the flow asymmetry occurs even for relatively small pressure differences, which differs from on-off valve-based systems where the pressure for backward flows typically diverges. To conclude, despite the simplicity of the current geometry, we observe a nonlinear flow asymmetry that is similar to that of the realistic channels discussed above.

C. Finite element simulations

To further investigate the origin of the flow nonlinearity and asymmetry, we simulate the flow and elastic deformations using a finite element 2D model (COMSOL 5.4) considering a Stokes flow and linear elastic approximation for the leaflets. The numerical simulation domain is a 2D channel of length $L = 40\,\text{mm}$ and width $h = 5.1\,\text{mm}$ that contains the 2D projections of one leaflet in its center [see Fig. 3(a)]. The length L is chosen long enough for the Poiseuille flow to fully develop before reaching the valve. The shape of the leaflet in the simulation is taken identical to the shape used in the experiment, and we considered the nonslip boundary conditions along the channel and

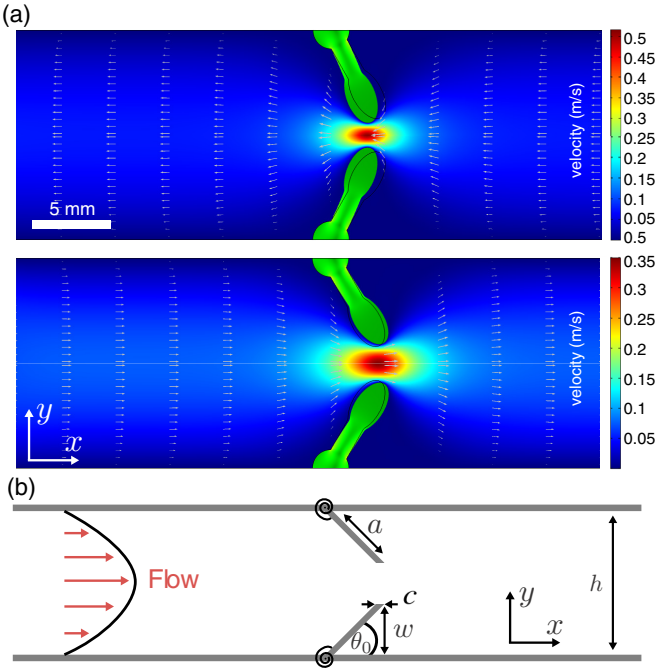

FIG. 3. Flow profile simulations and theoretical modeling. (a) 2D finite elements simulation of the flow field around soft leaflets with an initial angle $\theta_0 = 60^\circ$ at a flow rate $Q = 40\,\mathrm{ml/min}$. (b) Sketch of the theoretical model, where the leaflets are sketched as two rigid plates of length a with a ledge of length c and connected to the sides of the channel by torsion springs of stiffness k (black spirals).

the leaflets. To reduce calculation time, half of the system below or above the central axis of the channel is simulated by virtue of symmetry. The simulation box together with its mirrored image is shown in Fig. 3(a) for clarity. From the simulation, we quantify the deflection of the leaflet for different flow rates, which is in good agreement with the measurements on both rigid and soft leaflets [see Fig. 2(c), red and blue squares]. By matching the pressure obtained from the simulations and the experiments performed on the rigid leaflets [Fig. 2(d) blue circles and squares] with a correction factor $\beta = 2.3$, we also quantitatively capture the influence of the soft valve on the pressure-flow relationship [Fig. 2(d), red squares]. Therefore, although the 2D simulations do not take into account some 3D aspects of the experimental device such as the influence of the small gap between the leaflets and the top and bottom of the channel, they capture very well the fluid-structure interaction mechanism. In addition, the simulations guide us for construction of an even more idealized model described in the following.

D. Model

To capture the essence of the interaction between the fluid flow and the flexible leaflets, we model each leaflet as a thin and rigid plate of length a and angular position θ with a horizontal ledge of length c at its tip [see Fig. 3(b)]. The length of the ledge is chosen to be equal to the radius of curvature of the leaflet tip $c = 0.38$ mm, which allows to take into account the influence of the leaflets' thicknesses where the pressure is maximum within the channel. The compliance of the leaflets is modeled by a torsion spring connecting each leaflet to the rigid channel [black spirals in Fig. 3(b)], which is a reasonable assumption given the fact that elastic deformations of the leaflets are localized close to their anchoring points [see Fig. 2(b)]. The torsional stiffness $k = 33.5\,\mu\mathrm{N\,m/rad}$ was estimated from the valve Young's modulus, its length, and second moment of

area (see the Supplemental Material [28]). Given that the 2D finite element simulations capture well the experimental results, we model the flow around the leaflets as a 2D flow, therefore averaging the influence of the flow in the z direction, and rescale the pressure difference by the same correction factor used in the numerical simulations. We make the strong hypothesis of a parabolic flow profile between the two leaflets. As shown in the following lines and in the Supplemental Material [28], while this assumption deviates from the real flow profile, especially for straight leaflets, it allows for analytical predictions on the influence of the leaflets' geometry on the flow. The total pressure before the leaflets ($x = 0$) is expressed as

$$p = p_{\text{end}} + \frac{12\,\eta\beta q}{b}\left\{\int_0^{a\cos(\theta)} \frac{1}{[h - 2x\tan(\theta)]^3}dx + \int_0^{c} \frac{1}{[h - 2a\sin(\theta)]^3}dx\right\}, \tag{2}$$

where p_{end} is the pressure after the valve [$x = a\cos(\theta)$], q is the flow rate, η is the liquid viscosity, b is the channel's thickness, and β is the geometrical correction factor calibrated from the simulations. Equation (2) highlights the influence of both the bulk of the leaflets (first integral term) and the leaflets' tips (second integral term). For small values of θ, we expect the largest contribution to come from the bulk of the leaflets, while for θ near 90° we expect the main contribution to the pressure to come from the leaflets' tips. The equilibrium angle of the leaflets θ is set by the torque balance between the torque exerted by the flow on the leaflet and the elastic restoring torque of the leaflet,

$$b\int_0^{a\cos(\theta)} x\delta p(x)dx = k(\theta - \theta_0), \tag{3}$$

where k is the torsional stiffness, $\delta p(x)$ is the difference in pressure experienced by the leaflets at a point x on the leaflets, and θ_0 is the angle in the reference state (see the Supplemental Material [28]). Equations (2) and (3) demonstrate the very nature of the nonlinear fluid-structure interaction, where the flow deforms the structure [Eq. (3)], which in turn reconfigures the channel's geometry and affects the pressure difference [Eq. (2)]. We nondimensionalize Eqs. (2) and (3) by introducing the variables $\tilde{x} = x/L$, $\Delta\tilde{p}(x) = [p(x) - p_{\text{end}})/p_0$ and $\tilde{q} = q/q_0$, where $q_0 = bh^3p_0/(12\eta\beta a)$ and $p_0 = k/(ba^2)$. The new set of variables shows that the key parameters controlling the nonlinearity are the torsional stiffness k, the viscosity η, the length ratio h/a, and the initial angle θ_0. We numerically solve Eq. (3) to compute the position of the leaflets θ and from there inject θ in Eq. (2). The results are shown in the insets of Figs. 2(c) and 2(d) and are, without fitting parameters, in good agreement with the experiments and the simulations despite the simplicity of the model. To get a better understanding of the physics of the system, we solve Eqs. (2) and (3) perturbatively, in the limit of small deflections $(\theta - \theta_0) \ll 1$ and small flow rates $\tilde{q} \ll 1$. To leading order, the deflection $\theta - \theta_0$ evolves linearly with the flow:

$$\theta - \theta_0 = \tilde{q}[\mathrm{f}(\alpha_0)\cos^2(\theta_0)] + \left[\frac{\cos(\theta 0)}{T^2} + \frac{1}{2\,T^3}\right]\frac{\tilde{q}}{(1-\alpha_0)^3} + \mathcal{O}(\tilde{q}^2), \tag{4}$$

where $f(\alpha_0)$ is a function of $\alpha_0 = 2\sin(\theta_0)a/h$ and $T = c/a$ (see the Supplemental Material [28]). This linear expansion is consistent with the observation in Fig. 2(c) at small deflections. We then inject Eq. (4) into Eqs. (2) and (3), and we find that the difference in pressure between the leaflets is quadratic in the flow rate and thus have derived Eq. (1) from first principles (see the Supplemental Material for full derivation [28]). With this approach, we now have an analytical expression for the flow resistance R and the flow asymmetry ε (see the Supplemental Material [28]). From our complete description of the asymmetry generated by one pair of leaflets, combining experiments, simulation, and theoretical description, we can now efficiently explore the relationship between geometry and flow properties.

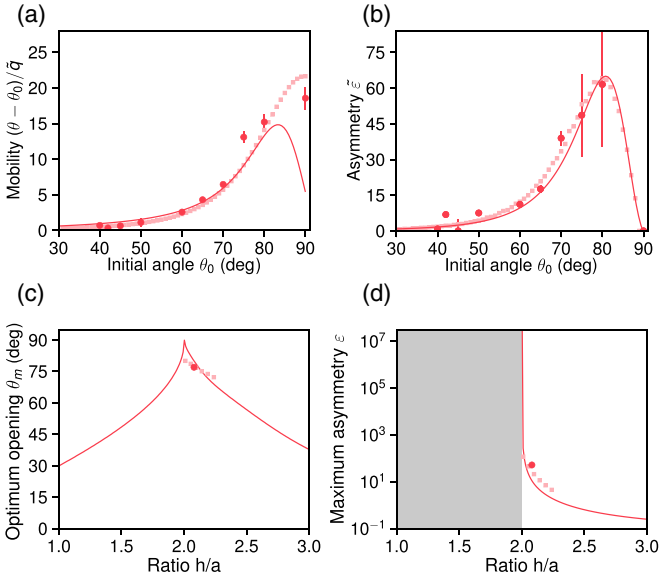

FIG. 4. Optimum leaflets geometry. (a) Mobility of the leaflet $(\theta - \theta_0)/\tilde{q}$ vs initial opening θ_0. (b) Flow asymmetry $\tilde{\varepsilon}$ vs initial angle θ_0. (c) Initial opening θ_m at which the flow asymmetry $\tilde{\varepsilon}$ is maximized vs geometric ratio h/a. (d) Corresponding maximum value of flow asymmetry vs aspect ratio h/a. The continuous lines correspond to the model. The red disks (squares) are obtained from quadratic fits to the experimental results (simulations). The error bars on the experimental results in panels (a), (b) correspond to the error on the linear and quadratic fits on the data.

E. Optimal geometry for maximal asymmetric flows

Which leaflet geometry does induce a maximally nonlinear and asymmetric flow? To address this question, we performed additional numerical simulations and experiments with different leaflet geometries. We first quantify the mobility $(\theta - \theta_0)/\tilde{q}$ of the leaflets in the limit of small flow rates as a function of the initial angle of the leaflets θ_0 [Fig. 4(b)]. The leaflet mobility monotonically increases with the angle θ_0. This result can be readily interpreted by a simple lever arm effect: The more transverse to the flow the leaflets are, the bigger the lever arm—hence the torque—of the fluid flow. Hence, channels with straighter leaflets—larger angles θ_0—will lead to a stronger fluid-structure interaction and more pronounced nonlinearities of the flow. To characterize the asymmetry of the pressure-flow relationship, we fitted Eq. (1) to the pressure-flow data. In Fig. 4(b), we plotted the nondimensionalized asymmetry $\tilde{\varepsilon} = \varepsilon\, q_0$ as a function of the initial angle θ_0 and show that ε varies nonmonotonically with the initial opening θ_0. For small initial angles θ_0, the leaflets are barely deformed by the liquid flow [Fig. 4(a)], leading to a linear pressure-flow-rate relationship and small flow asymmetry $\tilde{\varepsilon}$. As the initial angle increases, the valve is more deflected by the flow and the asymmetry between forward and backward flows increases. In contrast, a symmetric channel with an initial angle $\theta_0 = 90^\circ$ naturally has no flow asymmetry $\tilde{\varepsilon} = 0$. As a result, there is an optimum initial angle $\theta_0 = 80^\circ \pm 1^\circ$ at which the asymmetry between forward and backward flows is maximized and that results from a competition between geometry asymmetry and lever arm effects.

How does the optimal angle $\theta_0^{\max}$ and the corresponding flow asymmetry depend on the aspect ratio between the leaflet's length a and the channel width h? To answer this question, we use our numerical and theoretical models described above to explore different aspect ratio h/a [Fig. 4(c)]. For aspect ratios $h/a < 2$, i.e., leaflets longer than half the channel size, the maximal asymmetry is always obtained for leaflets that are initially touching, hence acting as an on-off valve. In this case,

the initial angle $\theta_0^{\max}$ maximizing the flow asymmetry can be simply derived from a geometric relation $\theta_0^{\max} = \arcsin[h/(2a)]$, which therefore decreases for smaller aspect ratios. In contrast, for aspect ratios $h/a > 2$, the geometrical balance is more intricate, and we find that for shorter leaflets, optimally nonlinear and asymmetric flows are obtained for more tilted leaflets [Fig. 4(c)]. We measured the level of asymmetry at the optimum angle for different ratios h/a [Fig. 4(d)]. For $h/a < 2$, any backward flow induces self-contact of the leaflets, triggering an on-off valve effect and leading to an infinite pressure and a theoretically infinite flow asymmetry $\tilde{\varepsilon}$. For $h/a > 2$ no such contact occurs, the pressure difference remains finite, and decreases with h/a. While it appears that maximum levels of asymmetry are reached for $h/a < 2$, note that the maximum of resistances R, defined in Eq. (1), also diverges at $h/a = 2$ (see the Supplemental Material [28]). Ratios $h/a > 2$ can therefore be optimum for systems that require small resistance R to generate flow.

Overall, our analytical prediction of the influence of the valve geometry on the flow is in good qualitative agreement with the experimental and numerical data without any fitting parameters, which indicates that our model has captured the essence of the flow asymmetry and can be used to predict optima of asymmetric leaflets. To further validate these analytical predictions, we used our analytical findings to describe the measurements performed on the leaflets with the lymphatic valve geometry [Fig. 1(a)]. We calibrated the minimum length a_{3D} in the center of the 3D leaflets and fitted with the analytical expression of ε the asymmetry measured in Fig. 1(c) with the torsional stiffness k as the only free parameter. The one parameter fit is in excellent agreement with the measurements for $k = 134\,\mu\mathrm{N\,m/rad}$, which is a good order of magnitude of the leaflet stiffness (see the Supplemental Material [28]). This result demonstrates the generality of our approach and its applicability to complex shapes. Furthermore, it rationalizes the *in vivo* observations of lymphatic valves with leaflets opened at rest [3,6].

To demonstrate that the asymmetry of the flow generated by the leaflets can be used to induce a pumping mechanism, analogous to that of the lymphatic system, we built an elementary circulatory system, described in Fig. 5(a). It is composed of a channel as described in Fig. 2(a), but which contains two pairs of leaflets. This rigid channel has three nozzles. The two lateral nozzles are connected to a soft tube while the third nozzle, situated in between the two pairs of leaflets is connected to a syringe pump. The syringe pump was programmed to cyclically inject and withdraw liquid within the closed system at a flow rate $Q = 50\,\mathrm{ml/min}$ and a frequency 0.25 Hz. As shown by Figs. 5(b) and 5(c), when liquid is injected (withdrawn), the soft tube expands (retracts), the left leaflets widen (narrow) the size of the channel, and the right leaflets narrow (widen) it. As a result, the clockwise flow is larger than the anticlockwise flow [see red arrows in Figs. 5(b) and 5(c). The image sequence in Figs. 5(d)–5(g) shows the experiment running for several periods. As the liquid is injected and withdrawn, we observe the clockwise displacement of bubbles (highlighted in red) situated within the deformable channel, which confirms that the flow oscillations are rectified to induce a net clockwise flow. The measurements of the right and left leaflets deflection in Fig. 5(h) confirms their asymmetric deformation, in accordance with our measurements on one pair of leaflets (see Fig. 2), and demonstrate that our initial observations of flow asymmetry performed in the case of stationary flows also apply to transient flows. The measurement of the bubble displacement in Fig. 5(i) confirms that the asymmetry in valve deflection leads to liquid transport: as liquid is injected and withdrawn, the bubbles move asymmetrically back and forth in the channel, with larger oscillations nearer to the leaflets. On average, the bubbles move forward in the channel with an average velocity of 5.7 mm/s, which demonstrates the simplicity of generating flow rectification and thus fluid transport using our asymmetric leaflets. Multiplying the average velocity of the bubble by the inner area of the soft tube, we obtain a unidirectional flow rate of 17.1 ml/min, corresponding to 34% of the oscillating flow rate. This observation is in direct agreement with our model of the valve asymmetry. From Eq. (1), we know that the unidirectional flow should be $\delta Q = \varepsilon Q_{\mathrm{in}}^2/2 = 18.9\,\mathrm{ml/min}$, which again confirms the ability of our model to predict the average flow asymmetry from the valve geometry even for oscillatory flows.

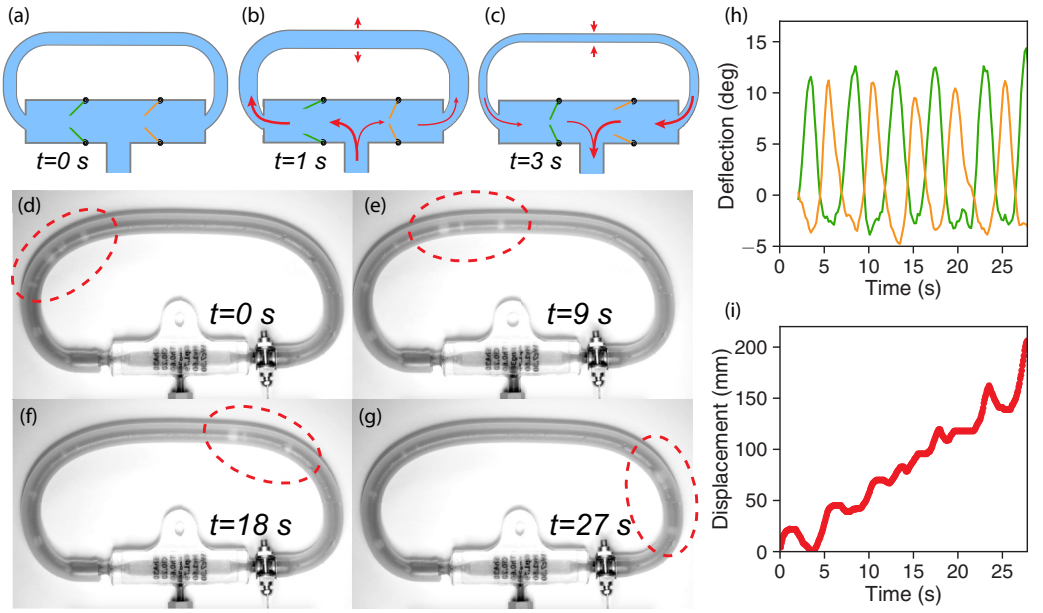

FIG. 5. Flow rectification mediated by asymmetric leaflets. (a)–(c) Schematic of the experiment composed of two pairs of leaflets connected to a soft tube and a syringe pump. When the syringe pump injects (withdraws) liquid in the closed channel, the tube expands (b) or retracts (c) and the leaflets deform asymmetrically. (d)–(g) Image sequence of bubbles (highlighted in red) moving clockwise in the soft tube due to the clockwise liquid transport. (h) Measurement of left (in green) and right (in orange) leaflet deflection over time. (i) The bubbles displacement over time, highlighting the overall displacement of the bubbles over several injections and suctions of liquid.

III. DISCUSSION

We have used bio-inspired soft leaflets to evidence a generic mechanism, where a nonlinear interaction between a laminar flow and a flexible structure induces a nonlinear and asymmetric flow response and flow rectification, i.e., converting oscillatory flows into fluid transport. These results are a first step in the modeling of the role of the leaflet geometry on internal flows in living systems such as lymphatic vessels. By going beyond empirical models previously developed [3,17] and associating the role of the leaflet shape on the flow asymmetry, our results might provide new ways to pinpoint the physical origin of lymph-related diseases. Indeed, we believe that the key parameters uncovered in this work, such as of the leaflet geometry and stiffness and the liquid rheology, are central to understanding the consequences of leaflet malformation, tissue weaknesses, or lymph properties on lymph transport malfunctions. In order to directly associate lymph-related diseases to each of those factors, this first work has to be further expanded with experiments involving active channel deformation and unsteady flows. Furthermore, similar measurements of the flow asymmetry ε and mobility should be performed *in vivo* as a function of the overall shape of the leaflet for specific specimens. The recent development of bio-printing of leaflets offers exciting ways to perform these next-step experiments [27].

Beyond biology, this research could open avenues, in terms of actuation process, autonomy, and cost, to current limitations in rapidly developing fields of research such as soft microfluidics [10,14,18–20] and soft robotics [21–26]. In particular, the current use of soft valves in microfluidics is limited to basic geometries and micropumps [30,31]. We envision that the use of asymmetric soft leaflets within channels could enable an unprecedented level of flow control. For instance, asymmetric leaflets could be employed to passively avoid backflows, open upon a given threshold,

or redirect flows toward specific junctions. To reach this objective, further experiments have to be performed at smaller scales, using other protocols such as UV-sensitive polymers [16] to assemble leaflets anchored in microchannels and studies have to be performed on multichannel systems containing numerous leaflets in order to quantify the interaction between leaflets and their influence on flows at junctions.

ACKNOWLEDGMENTS

We are grateful to T. Gilet and A. Schiphorst for insightful discussions. We thank D. Giesen, S. Koot, and G. Hardeman for skillful technical support, and L. D. Thanh, A. Schiphorst, E. Peerbooms, and S. Broersen for preliminary experiments. We acknowledge funding from the European Research Council, through the Starting Grant No. 852587.

M.B. and C.C. designed the research. M.B. and A.D. performed the experiments and developed the theoretical model, M.B and R.S. performed the numerical simulations, and M.B and C.C. wrote the manuscript; all authors discussed the result and commented on the manuscript.

[1] S. Vogel, *Cats' Paws and Catapults: Mechanical Worlds of Nature and People* (W. W. Norton & Company, New York, 2000).

[2] F. Sotiropoulos, T. B. Le, and A. Gilmanov, Fluid mechanics of heart valves and their replacements, Annu. Rev. Fluid Mech. **48**, 259 (2016).

[3] J. E. Moore and C. D. Bertram, Lymphatic system flows, Annu. Rev. Fluid Mech. **50**, 459 (2018).

[4] M. Y. Jaffrin and A. H. Shapiro, Peristaltic pumping, Annu. Rev. Fluid Mech. **3**, 13 (1971).

[5] C. Kunert, J. W. Baish, S. Liao, T. P. Padera, and L. L. Munn, Mechanobiological oscillators control lymph flow, Proc. Natl. Acad. Sci. USA **112**, 10938 (2015).

[6] D. C. Zawieja, Contractile physiology of lymphatics, Lymphatic Res. Biol. **7**, 87 (2009).

[7] P. Guo, A. M. Weinstein, and S. Weinbaum, A hydrodynamic mechanosensory hypothesis for brush border microvilli, Am. J. Physiol. - Renal Physiol. **279**, F698 (2000).

[8] E. A. Schwartz, M. L. Leonard, R. Bizios, and S. S. Bowser, Analysis and modeling of the primary cilium bending response to fluid shear, Am. J. Physiol. - Renal Physiol. **272**, F132 (1997).

[9] J. S. Wexler, P. H. Trinh, H. Berthet, N. Quennouz, O. du Roure, H. E. Huppert, A. Lindner, and H. A. Stone, Bending of elastic fibres in viscous flows: the influence of confinement, J. Fluid Mech. **720**, 517 (2013).

[10] M. Gomez, D. E. Moulton, and D. Vella, Passive Control of Viscous Flow via Elastic Snap-Through, Phys. Rev. Lett. **119**, 144502 (2017).

[11] K. Park, A. Tixier, A. H. Christensen, S. F. Arnbjerg-Nielsen, M. A. Zwieniecki, and K. H. Jensen, Viscous flow in a soft valve, J. Fluid Mech. **836**, R3 (2018).

[12] *Fluid-Structure Interactions in Low-Reynolds-Number Flows*, edited by C. Duprat and H. Stone, Soft Matter Series (The Royal Society of Chemistry, London, 2016), pp. P001–477.

[13] A. Amir, F. Babaeipour, D. B. McIntosh, D. R. Nelson, and S. Jun, Bending forces plastically deform growing bacterial cell walls, Proc. Natl. Acad. Sci. USA **111**, 5778 (2014).

[14] J. Alvarado, J. Comtet, E. de Langre, and A. E. Hosoi, Nonlinear flow response of soft hair beds, Nat. Phys. **13**, 1014 (2017).

[15] J.-D. Julien and K. Alim, Oscillatory fluid flow drives scaling of contraction wave with system size, Proc. Natl. Acad. Sci. USA **115**, 10612 (2018).

[16] J. Cappello, M. Bechert, C. Duprat, O. du Roure, F. Gallaire, and A. Lindner, Transport of flexible fibers in confined microchannels, Phys. Rev. Fluids **4**, 034202 (2019).

[17] A. S. Jamalian, M. Jafarnejad, S. D Zawieja, C. D Bertram, A. Gashev, D. C. Zawieja, M. J. Davis, and J. E. Moore, Demonstration and analysis of the suction effect for pumping lymph from tissue beds at subatmospheric pressure, Sci. Rep. **7**, 12080 (2017).

[18] M. A. Unger, H.-P. Chou, T. Thorsen, A. Scherer, and S. R. Quake, Monolithic microfabricated valves and pumps by multilayer soft lithography, Science **288**, 113 (2000).
[19] D. P. Holmes, B. Tavakol, G. Froehlicher, and H. A. Stone, Control and manipulation of microfluidic flow via elastic deformations, Soft Matter **9**, 7049 (2013).
[20] B. Tavakol, M. Bozlar, C. Punckt, G. Froehlicher, H. A. Stone, I. A. Aksay, and D. P. Holmes, Buckling of di electric elastomeric plates for soft, electrically active microfluidic pumps, Soft Matter **10**, 4789 (2014).
[21] N. Vasios, A. J. Gross, S. Soifer, J. T. B. Overvelde, and K. Bertoldi, Harnessing viscous flow to simplify the actuation of fluidic soft robots, Soft. Robot. **7**, 1 (2019).
[22] M. Wehner, R. L. Truby, D. J Fitzgerald, B. Mosadegh, G. M. Whitesides, J. A. Lewis, and R. J. Wood, An in tegrated design and fabrication strategy for entirely soft, autonomous robots, Nature **536**, 451 (2016).
[23] L. Hines, K. Petersen, G. Z. Lum, and M. Sitti, Soft actuators for small-scale robotics, Adv. Mater. **29**, 1603483 (2017).
[24] P. Polygerinos, N. Correll, S. A. Morin, B. Mosadegh, C. D. Onal, K. Petersen, M. Cianchetti, M. T. Tolley, and R. F. Shepherd, Soft robotics: Review of fluid-driven intrinsically soft devices; manufacturing, sensing, control, and applications in human-robot interaction, Adv. Eng. Mater. **19**, 1700016 (2017).
[25] P. Rothemund, A. Ainla, L. Belding, D. J. Preston, S. Kurihara, Z. Suo, and G. M. Whitesides, A soft, bistable valve for autonomous control of soft actuators, Sci. Rob. **3**, eaar7986 (2018) .
[26] J. T. B. Overvelde, T. Kloek, J. J. A. D'haen, and K. Bertoldi, Amplifying the response of soft actuators by harnessing snap-through instabilities, Proc. Natl. Acad. Sci. USA **112**, 10863 (2015).
[27] B. Grigoryan, S. J. Paulsen, D. C. Corbett, D. W. Sazer, C. L. Fortin, A. J. Zaita, P. T. Greenfield, N. J. Calafat, J. P. Gounley, A. H. Ta, F. Johansson, A. Randles, J. E. Rosenkrantz, J. D. Louis-Rosenberg, P. A. Galie, K. R. Stevens, and J. S. Miller, Multivascular networks and functional intravascular topologies within biocompatible hydrogels, Science **364**, 458 (2019).
[28] See Supplemental Material at http://link.aps.org/supplemental/10.1103/PhysRevFluids.5.084102 for a detailed description of the lymphatic leaflet geometry and the derivation of the outflows associated, and a detailed description of the 2D leaflets geometry and the theoretical model associated.
[29] M. Heil and A. L Hazel, Fluid-structure interaction in internal physiological flows, Annu. Rev. Fluid Mech. **43**, 141 (2011).
[30] K. W. Oh and C. H. Ahn, A review of microvalves, J. Micromech. Microeng. **16**, 13 (2006).
[31] S. Mohith, P. Navin Karanth, and S. M. Kulkarni, Recent trends in mechanical micropumps and their applications: A review, Mechatronics **60**, 34 (2019).